Journal of Hazardous Materials 192 (2011) 255–262

Contents lists available at ScienceDirect

Journal of Hazardous Materials

journal homepage: www.elsevier.com/locate/jhazmat

Silica materials recovered from photonic industrial waste powder: Its extraction, modification, characterization and application

Liang-Yi Lin, Jien-Ting Kuo, Hsunling Bai*

Institute of Environmental Engineering, National Chiao Tung University, 1001 University Rd., Hsinchu 300, Taiwan

ARTICLE INFO

Article history:
Received 2 February 2011
Received in revised form 3 May 2011
Accepted 5 May 2011
Available online 11 May 2011

Keywords:
Resource recovery
Photonic industrial waste powder
Mesoporous silica materials
CO_2 adsorbent

ABSTRACT

This study explored the possibility of recovering waste powder from photonic industry into two useful resources, sodium fluoride (NaF) and the silica precursor solution. An alkali fusion process was utilized to effectively separate silicate supernatant and the sediment. The obtained sediment contains purified NaF (>90%), which provides further reuse possibility since NaF is widely applied in chemical industry. The supernatant is a valuable silicate source for synthesizing mesoporous silica material such as MCM-41. The MCM-41 produced from the photonic waste powder (PWP), namely MCM-41(PWP), possessed high specific surface areas (1082 m^2/g), narrow pore size distributions (2.95 nm) and large pore volumes (0.99 cm^3/g). The amine-modified MCM-41(PWP) was further applied as an adsorbent for the capture of CO_2 greenhouse gas. Breakthrough experiments demonstrated that the tetraethylenepentamine (TEPA) functionalized MCM-41(PWP) exhibited an adsorption capacity (82 mg CO_2/g adsorbent) of only slightly less than that of the TEPA/MCM-41 manufactured from pure chemical (97 mg CO_2/g adsorbent), and its capacity is higher than that of TEPA/ZSM-5 zeolite (43 mg CO_2/g adsorbent). The results revealed both the high potential of resource recovery from the photonic solid waste and the cost-effective application of waste-derived mesoporous adsorbent for environmental protection.

1. Introduction

Since the evolution of computer science and information technology, demands on large scale silicon integrated circuit processes increase rapidly during recent years. However, huge amounts of waste products have been created in the forms of waste solvents, sludge and solid waste, etc. Silicon (Si)-containing waste powder is a common waste product of chemical vapor deposition (CVD) process in thin film transistor-liquid crystal display (TFT-LCD) and semiconductor plants. In a typical CVD process, gaseous reagents of silane (SiH_4) and ammonia (NH_3) are introduced and silicon derived compounds such as silica and/or silicon nitride (SiN_X) thin films are formed on the substrates. The cleaning agent of nitrogen trifluoride (NF_3) is subsequently introduced to clean up the accumulative particles formed on the wall of the reaction chamber. The waste powders are then collected by baghouses located in the exhaust of the CVD process. Such waste powders are light-density with bulky volume and are thus difficult to be transported and disposed of. Therefore, additional expenses on waste treatment and landfill disposal are needed.

Waste recovery is an effective strategy to avoid the fast drain of natural resources. This has been especially important on using the natural resources for the capture of abundant CO_2 greenhouse gas. For example, silica materials have been tested [1] for their potential as adsorbents on capturing CO_2. However, such silica adsorbents were mainly made from pure chemical sources, which have been in shortage due to large demands of silicon in semiconductor, photonic and solar cell industries, etc.

The periodic mesoporous silica materials received tremendous attention since the first discovery by Mobil oil researchers [2]. These mesoporous silica materials with high surface area (>1000 m^2/g), narrow pore distribution and well-defined pore structures are useful in the application fields of catalysis and adsorption [3,4]. Generally, such materials can be synthesized using various sources of silica, including expensive organic precursors such as silicon alkoxides [5] and cost-effective reagents like colloidal silica and sodium silicate [6]. The use of cheaper silica source instead of expensive silica precursor in the synthesis process would be a great contribution to industrial applications, especially for the environmental protection applications which require massive quantity of adsorbents or catalysts.

Recently, several research studies have attempted to reuse solid wastes for manufacturing mesoporous silica materials. This includes coal fly ash [7] and rice husk ash [8] which are by-products of the coal-fired power plant and agricultural activities, respectively. Chang et al. [9] firstly synthesized mesoporous aluminosiliicate using fly ash as the precursor. The results confirmed the presence of hexagonal pore arrangement with a high surface

* Corresponding author. Tel.: +886 3 5731868; fax: +886 3 5725958.
E-mail addresses: hlbai@mail.nctu.edu.tw, hlbai@green.ev.nctu.edu.tw (H. Bai).

0304-3894/$ – see front matter © 2011 Elsevier B.V. All rights reserved.
doi:10.1016/j.jhazmat.2011.05.011

area of 735 m^2/g. Besides, Hui and Chao [7] reported the effects of synthesis parameters on the mesostructure of Si-MCM-41 with the supernatant of the coal fly ash as the precursor solution. They demonstrated the effect of initial pH value on the incorporation amounts of Ti, Al and Fe species during the synthesis.

Unlike the coal fly ash or rice husk ash which contains lots of complicated metal oxides [10,11], the primary components of photonic waste powder might only contain Si-, N- and F-species. Thus it would be more facile to be utilized as the silica source since high purity of silica could be obtained. To the authors' knowledge, the identification of the waste powder from CVD processes of either semiconductor or photonic industry as well as the possibility of waste powder recovery for further environmental applications have not been reported yet.

In the present investigation, attempts have been made to evaluate the chemical composition of the photonic waste powder as well as to recover the supernatant and the sediment into valuable resources. The supernatant is used as the silica source for the synthesis of MCM-41. The chemical composition, pore structure, morphology as well as CO_2 adsorption performance of the obtained MCM-41 from the photonic waste powder are presented and compared with those of the MCM-41 obtained from pure chemical. In order to understand the industrial applicability, the performance of these two mesoporous materials are also compared to that of the commercial ZSM-5 zeolite adsorbent for adsorbing CO_2 greenhouse gas.

2. Experimental

2.1. Waste powder characterization and extraction

The photonic waste powder was obtained from a TFT-LCD plant and characterized without any pretreatment. The elemental analysis of the waste powder was determined by energy-dispersive X-ray spectroscopy in a scanning electron microscope (SEM-EDS, HITACHI-S4700). The functional groups of the waste powder were characterized by the FTIR instrument (Bruker Vector 22 IR). Powder low angle X-ray diffraction pattern of the waste powder was recorded by Rigaku X-ray diffractometer equipped with nickel-filtered CuKα (λ = 1.5405 Å) radiation. The diffractogram was recorded in the 2θ range of 5–80° with a scanning speed of 2° per minute. The specific surface area, pore volume and average pore diameter (BJH method) of the sample were measured by N_2 adsorption–desorption isotherms at −196 °C using a BET surface area analyzer (Micromeritics, ASAP 2000). The thermal behavior of the waste powder was determined in the temperature range of 25–900 °C using a thermo-gravimetric analyzer (TGA, Netzsch TG209 F1, Germany).

The extraction of silica was carried out through an alkali fusion treatment [9]. In a typical process, the waste powder and NaOH powder were thoroughly mixed at a weight ratio of 1:1.2 and fused at 550 °C for 1 h. The received fused product was then mixed with DI water at a weight ratio of 1:5 with continuous stirring for 24 h. The resulting mixture was then centrifuged to separate the sediment for further characterization of its components. And the supernatant was also analyzed by ICP-MS (SCIEX ELAN 5000 – Inductively Coupled Plasma-Mass Spectrometer) and utilized for the synthesis of MCM-41.

2.2. Synthesis and characterization of the mesoporous silica MCM-41

Mesoporous silica materials of MCM-41 were synthesized by hydrothermal treatment method using either waste derived silica or pure silica source as the precursor solutions. Cetyltrimethylammonium bromide (CTAB) was employed as the structure-directing template in the synthesis. For the photonic waste derived MCM-41, the molar composition of the gel mixture was 1 SiO_2:0.2 CTAB:0.89 H_2SO_4:120 H_2O, where the SiO_2 precursor source was obtained from the supernatant of photonic waste powder extraction process described in Section 2.1. In a typical synthesis procedure, 50 ml of supernatant was firstly stirred vigorously for 30 min. Then, the pH of the solution was adjusted to 10.5 using 2 M H_2SO_4 followed by further stirring to form a gel. After that 4.6 g of CTAB (dissolved in 16 ml of DI water) was added drop by drop into the above mixture and the combined mixture was stirred for three additional hours. The resulting gel mixture was transferred into a Teflon coated autoclave and kept in an oven at 145 °C for 36 h. After cooling to room temperature, the resultant solid was recovered by filtration, washed with DI water and dried in an oven at 110 °C for 6 h. Finally, the organic template was removed via a muffle furnace in air at 550 °C for 6 h. The MCM-41 material synthesized from photonic waste powder (PWP) was named as MCM-41(PWP).

For comparison purpose, the synthesis of MCM-41 using pure sodium metasilicate nanohydrate ($Na_2SiO_3{\cdot}9H_2O$) was also performed following similar procedure described previously for the synthesis of MCM-41(PWP). The detailed procedure was described in Karthik et al. [12]. The molar composition of the gel mixture was 1 SiO_2:0.2 CTAB:120 H_2O:0.89 H_2SO_4. The MCM-41 material derived from pure chemical of $Na_2SiO_3{\cdot}9H_2O$ was denoted as MCM-41(NaSi).

The calcined MCM-41 materials were characterized by BET surface area analyzer, XRD analysis and the EDS instrument as described previously for the characterization of photonic waste powders. In addition, TEM images of the calcined MCM-41 materials were obtained with a TEM instrument (JEOL JEM 1210) operated at 120 keV and the samples (5–10 mg) were ultrasonicated in ethanol and dispersed on carbon film supported on copper grids (200 mesh).

2.3. TEPA-impregnated MCM-41 for CO_2 capture

In order to enhance the adsorption performance for the capture of CO_2, all adsorbents (MCM-41(PWP), MCM-41(NaSi) and ZSM5 zeolite) were modified with the amine agent of tetraethylenepentamine (TEPA) at a weight ratio of 1:1 by the wet impregnation method described in Lu et al. [13]. To obtain the adsorption capacity and breakthrough curve of the adsorbents, CO_2 adsorption experiment was carried out in a packed column with an internal diameter of 0.75 cm. The adsorption column was packed with 1.0 g of adsorbents (packing height = ~5 cm) and placed in a temperature-controlled oven. In a typical process, adsorbents were pretreated under a N_2 flow of 0.2 L/min at 110 °C for 1 h, and then cooled to 25 °C. Subsequently, the gas flow was switched to 20% (v/v) CO_2 gas stream (balanced with N_2) under a flow rate of 0.1 L/min. The concentration of CO_2 was continuously measured by a CO_2 analyzer (Molecular Analytics AGM 4000 Gas Analyzer). The CO_2 adsorption capacity (q, mg/g) at a certain time (t, time) was estimated as

$$q = \frac{1}{m}\int_0^t Q \times (C_{in} - C_{eff})dt \quad (1)$$

where m is the weight of adsorbent (g), Q is the gas flow rate (L/min), and C_{in} and C_{eff} are the influent and effluent CO_2 concentrations (mg/L), respectively, which are expressed in terms of percent in volume (%). The adsorption capacity of zero gas (N_2 only) was deducted from the adsorption capacities of adsorbents.

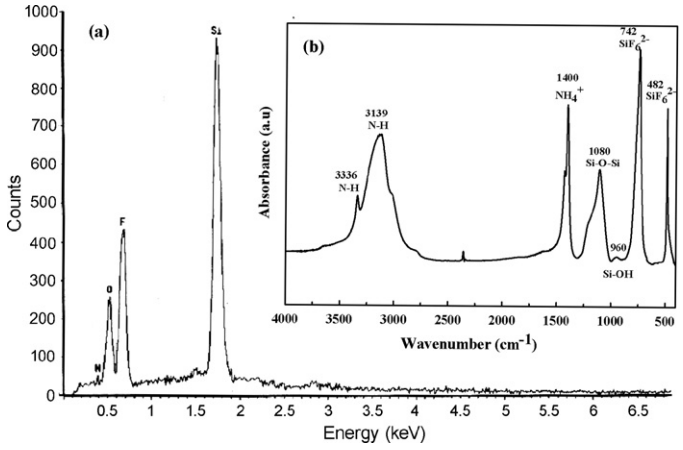

Fig. 1. (a) EDS spectrum and (b) FTIR spectrum of the photonic waste powder.

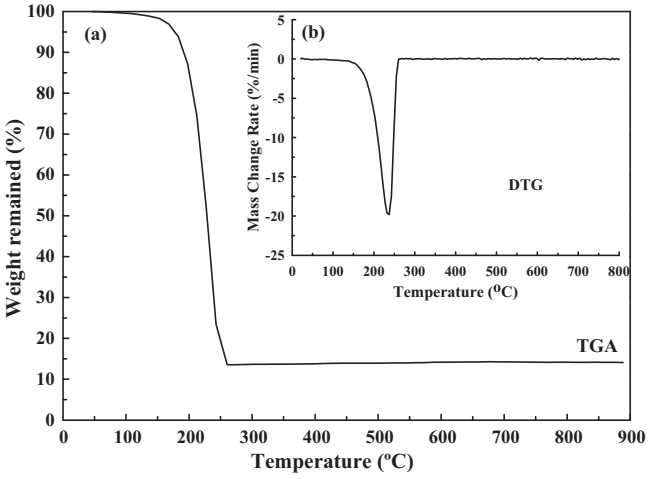

Fig. 3. (a) TGA analysis and (b) DTG profile of the photonic waste powder.

3. Results and discussion

3.1. Characterization of the photonic waste powder (PWP)

The results of EDS and FTIR analyses for the photonic waste powder are shown in Fig. 1, and the weight percentages of each element in the photonic waste powder are listed in Table 1. As can be seen from Fig. 1a, the four observed elements of Si, O, N and F in the photonic waste powder were expected since the solid waste was derived from the CVD process in which the three gaseous reactants were SiH_4, NF_3 and NH_3. Furthermore, the FTIR spectrum of photonic waste powder shown in Fig. 1b exhibited significant absorption bands at 3336, 3139, 1400, 1080, 960, 742 and 482 cm^{-1}. The bands at 3336 and 3139 cm^{-1} are related to N–H stretching, while 742 and 482 cm^{-1} can be assigned to SiF_6^{2-} [14]. Besides, the bands at 1400, 1080 and 960 cm^{-1} can be assigned to the NH_4^+ [14], Si–O–Si and Si–OH stretching vibrations, respectively [15]. Considering the above results, the primary components in photonic waste powder could be the admixture of $(NH_4)_2SiF_6$ and SiO_2.

The XRD analysis was then carried out to further identify the crystalline components in the photonic waste powder with the result depicted in Fig. 2. Strong $(NH_4)_2SiF_6$ diffraction peaks were identified [16]. In contrast, the diffraction peak of silica was not observed from the XRD pattern, suggesting that SiO_2 was only present in little amount and it might be trapped in the $(NH_4)_2SiF_6$ lattice. However the precise weight percentages of $(NH_4)_2SiF_6$ and SiO_2 could not be obtained from Table 1 since the EDS data only provided a rough estimate of the elemental content, while the ICP-MS could only detect the Si content in the photonic waste powder.

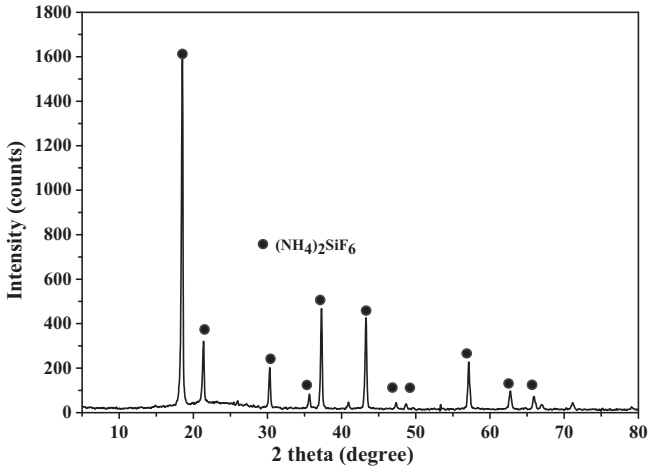

Fig. 2. XRD pattern of the photonic waste powder.

The weight percentages of $(NH_4)_2SiF_6$ and SiO_2 presented in the photonic waste powder were determined using TGA weight loss and differential thermo-gravimetric (DTG) analyses. It can be seen from Fig. 3a that the photonic waste powder sample showed an initial weight loss at <150 °C, which could be ascribed to the evaporation of the physically adsorbed water on the surface of the materials. As the temperature exceeded 150 °C, there was a significant weight loss for the photonic waste powder at around 237 °C as clearly observed from Fig. 3b. Mel'nichenko et al. [17] investigated the mechanism of the solid-phase reaction between $(NH_4)_2SiF_6$ and SiO_2, and proposed that $(NH_4)_2SiF_6$ could be thermally decomposed between 220 and 300 °C in the presence of SiO_2. Generally, the following chemical reactions are expected to take place when $(NH_4)_2SiF_6$ was heated up to 900 °C [16]:

$$(NH_4)_2SiF_6 \xrightarrow{220\,^\circ C} SiF_{4(g)} + 2NH_4F_{(s)} \quad (2)$$

$$NH_4F_{(s)} \xrightarrow{850\,^\circ C} NH_4F_{(g)} \quad (3)$$

Considering the above reactions, $(NH_4)_2SiF_6$ would be completely decomposed during the thermal treatment up to 900 °C. However, it is noted that there was still 15 wt.% of residues remained after heating up the photonic waste powder to 900 °C. This is probably due to the presence of SiO_2 since it is thermally stable up to 900 °C. The total Si weight fraction (from $(NH_4)_2SiF_6$ and SiO_2) of 20.4% calculated by the TGA/DTG result was very close to the Si mass fraction of 22.4% detected by the ICP-MS result shown in Table 1. Therefore, the primary components in photonic waste powder were determined to be around 85% of $(NH_4)_2SiF_6$ and 15% of SiO_2 from the results of TGA, FTIR and SEM-EDS analysis.

3.2. Characterization of sediment and supernatant liquid after extraction

Fig. 4 shows the EDS spectrum of the sediment and its corresponding XRD pattern. It can be found from Fig. 4a that Na and F were the primary elements in the sediment, with negligible Si and O species, which was also confirmed by the result of EDS analysis shown in Table 1. The residual SiO_2 could be due to insufficient NaOH amounts applied in the extraction process. The major component of NaF presented in the sediment was also demonstrated by

Table 1
Elemental analysis of photonic waste powder and sediment analyzed by the SEM-EDS and ICP-MS analyses.

Element	Si	F	O	N	Na
Photonic waste powder (wt.%)[a]	28.82	47.82	17.54	5.82	–
Sediment (wt.%)[a]	5.22	33.34	2.99	–[c]	58.45
Photonic waste powder (wt.%)[b]	22.35	–	–	–	–
Supernatant (ppm)[b]	13,080	–	–	–	33,180

[a] Sample analyzed by the SEM-EDS analysis.
[b] Sample analyzed by the ICP-MS analysis.
[c] Not detected.

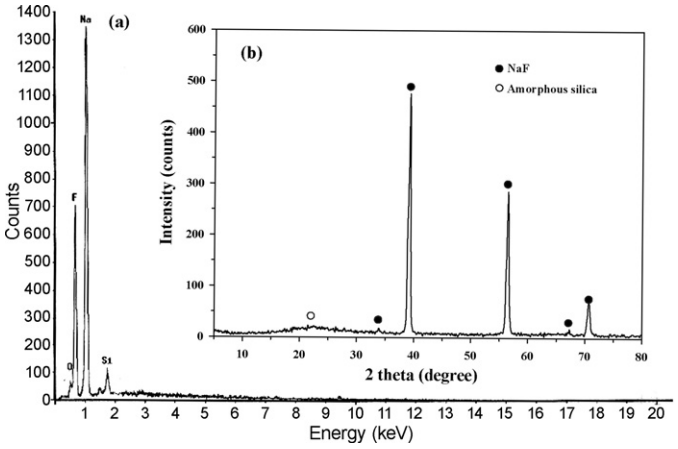

Fig. 4. (a) EDS spectrum and (b) XRD pattern of the sediment after silica extraction.

Fig. 4b. The five sharp diffraction peaks located at 34, 39, 56, 67 and 70.5° were in agreement with the NaF standard XRD peaks [18,19]. Besides, there was a broad peak centering at 22° as observed from Fig. 4b, which can be ascribed to the amorphous SiO_2 [20]. This result is consistent with the EDS spectrum which showed that Si and O species were also presented in minor amounts.

The thermal behavior of the sediment was subsequently investigated using TGA and DTG analyses. It can be seen from Fig. 5a that there was only around 5% weight loss for the sediment during the thermal treatment up to 900 °C. The DTG curve showed three distinguished peaks from room temperature to 900 °C (Fig. 5b). The first step (<150 °C) is due to the loss of physically adsorbed water on the surface of the sediment and the second step (150–600 °C) is attributed to the loss of chemically adsorbed water bonded to Si–OH through hydrogen bond [21] since the sediment contained only a little amount of SiO_2. From 600 to 900 °C, the weight loss is expected to be associated with the further condensation of the Si–OH groups from the amorphous SiO_2 [20].

As a result, one can conclude that F was effectively captured by NaOH and the sodium fluoride (NaF) sediments were formed after the extraction process. The NaF purity was quite high (>90%) in the sediment as observed from the TGA/DTG data, which provides further possibility for reuse. Sodium fluoride is one of the well-known chemical compounds which are widely utilized in industries as the source of fluoride ion in diverse applications. In other words, the photonic waste powder can be converted into two valuable resources, the supernatant as the silica precursor and the sediment of sodium fluoride.

The composition of the supernatant was also analyzed by ICP-MS in order to investigate the concentrations of Si and Na ions. Table 1 shows that the concentrations of Si and Na ions were 13,080 and 33,180 ppm, respectively. The concentration ratio between Na and Si is 2.54 in this study. It is lower than the Na/Si ratio of silica supernatant recovered from fly ash [9] in which the Si and Na concentrations were 572 and 12,000 ppm, respectively. Chang et al. [9] stated that the high concentration ratio of Na/Si in the precursor tended to hinder the mesostructure and thus the MCM-41 obtained from fly ash supernatant could not exceed 1000 m^2/g. In comparison, the silica supernatant obtained from the photonic waste powder could be a better source for producing high quality waste-derived MCM-41.

3.3. Characterization of MCM-41(PWP)

Fig. 6a shows the EDS spectrum of the MCM-41 sample synthesized from the photonic waste powder. It can be seen that only Si and O elements were present in MCM-41(PWP) indicating that alkali fusion treatment is a viable process to effectively separate silicate species from the PWP derived silica. Fig. 6b illustrates the

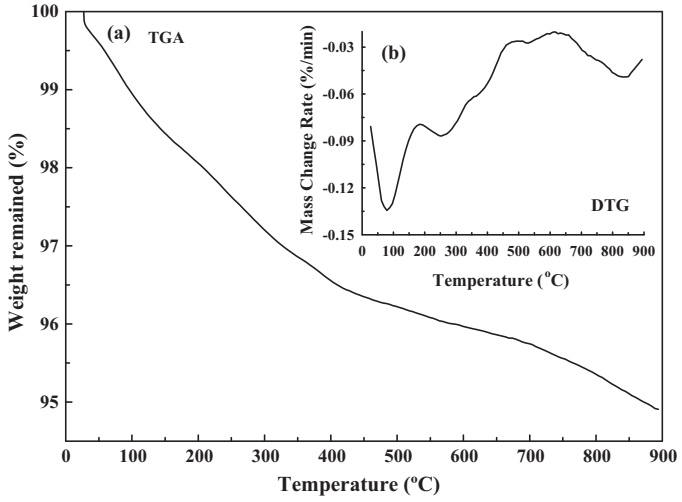

Fig. 5. (a) TGA analysis and (b) DTG profile of the sediment.

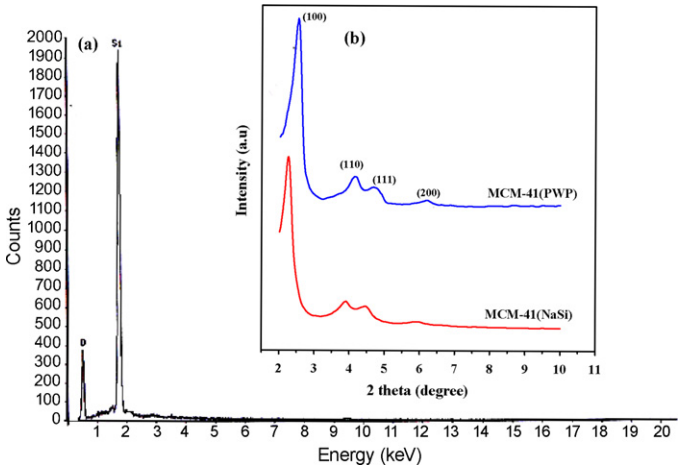

Fig. 6. (a) EDS spectrum of MCM-41(PWP) sample and (b) XRD patterns of the MCM-41(PWP) and MCM-41(NaSi) samples.

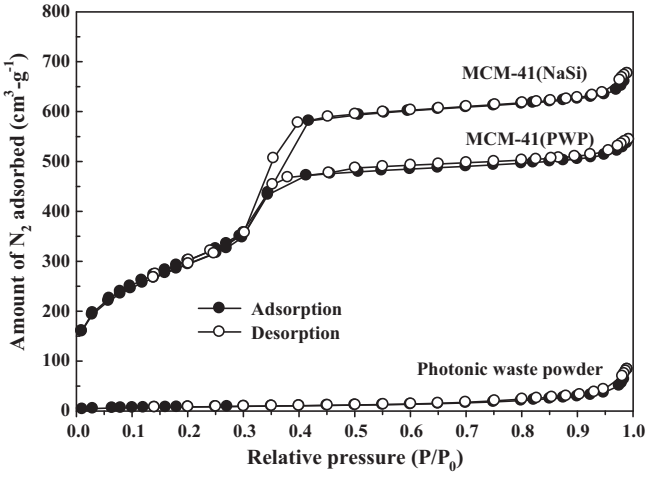

Fig. 7. N_2 adsorption–desorption isotherms of the photonic waste powder, calcined MCM-41(NaSi) and MCM-41(PWP) samples.

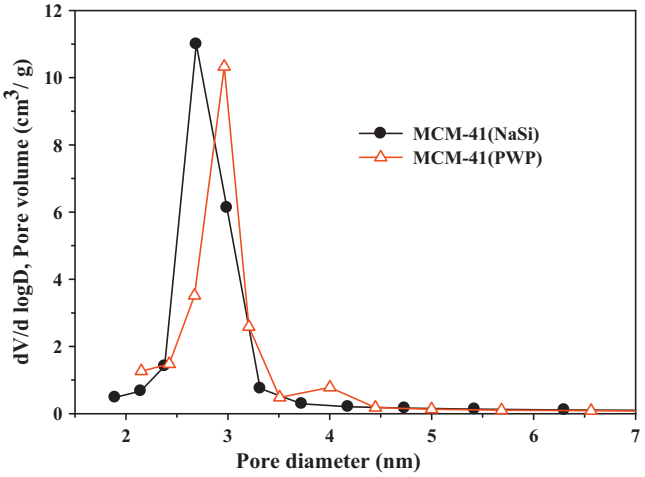

Fig. 8. BJH pore diameter distributions of calcined MCM-41(NaSi) and MCM-41(PWP) samples.

powder XRD patterns of the MCM-41(PWP) and MCM-41(NaSi) samples. One can see that MCM-41(NaSi) sample exhibited a well-defined (1 0 0) diffraction peak located at 2θ of 2.3–2.6° and three reflections of (1 1 0), (2 0 0) and (2 1 0) at 4.2, 4.7 and 6.2°, respectively, which could be indexed on a hexagonal lattice of mesoporous silica materials [6,12,22]. Similar observation was also seen for the MCM-41(PWP) sample, thus indicating that highly ordered mesostructure was obtained using the supernatant extracted from photonic waste powder as the silica source.

The N_2 adsorption–desorption isotherms of photonic waste powder, MCM-41(NaSi) and MCM-41(PWP) are shown in Fig. 7. It is clear that photonic waste powder exhibited a typical type II isotherm of non-porous materials according to the IUPAC classification. On the other hand, both MCM-41(NaSi) and MCM-41(PWP) possessed type IV isotherms which are the characteristic of mesoporous materials, featuring a narrow step due to capillary condensation of N_2 within the primary mesopores [5,23]. The isotherms of the MCM-41(NaSi) and MCM-41(PWP) also showed the type H1 hysteresis loop associated with well-arranged cylindrical channels with uniform shape and pore size [24]. However, the less steep condensation step for MCM-41(PWP) sample indicates a lesser degree of uniform mesostructure as compared to that of MCM-41(NaSi) sample. This was expected since the silica precursor of MCM-41(PWP) could not be in such a high purity as the pure chemical of Na_2SiO_3 for producing MCM-41(NaSi).

Fig. 8 displays the BJH pore size distributions of MCM-41(NaSi) and MCM-41(PWP) samples. It is clear that MCM-41(NaSi) sample showed a narrow pore size distribution with the peak pore size at 2.7 nm, suggesting the uniform porosity of the obtained materials. The MCM-41(PWP) also showed a narrow pore size distribution with the peak size at around 3.0 nm. But a small peak located at around 4 nm was also observed. The bimodal mesoporosity would result in less uniformity of mesostructure of MCM-41(PWP).

The physicochemical properties of BET specific surface area, specific pore volume and average pore diameter derived from the N_2 adsorption–desorption measurements are summarized in Table 2. To check the stability of using the photonic waste powder for preparing the MCM-41(PWP), duplicate experiments were performed and the BET characterization of the two MCM-41(PWP) samples prepared from two different batches of waste powder showed that there was negligible effect on the sample pore structure. This could be attributed to the fact that the solid waste powder was obtained from the same TFT-LCD plant, which controls their process precisely and stably. It can be observed that MCM-41(PWP) possessed high specific surface area (1082 m^2/g), narrow pore size distribution (2.95 nm) and large pore volume (0.99 cm^3/g) which are fairly closed to the properties of MCM-41(NaSi). The slight shrinkage in the pore volume of MCM-41(PWP) could be due to the higher amounts of Na ions in the supernatant [9]. However, the effect of the higher Na concentration was very minor which could be attributed to precise pH-controls during the synthesis of the MCM-41(PWP).

The textural mesostructure of the MCM-41(NaSi) and MCM-41(PWP) samples was further revealed by TEM images shown in Fig. 9a and b, respectively. The TEM image of MCM-41(PWP) material (Fig. 9b) clearly shows a well ordered long range hexagonal array of mesopores similar to that of the MCM-41(NaSi) material (Fig. 9a), and these long range crystallographic features are consistent with the results of XRD and BET analyses. The pore diameter observed in Fig. 9b was ca. 3.2 nm which was fairly close to the narrow pore size distribution (BJH) determined by N_2 adsorption–desorption measurements, indicating that the pore structure of MCM-41(PWP) is highly ordered.

3.4. Application as adsorbents for CO_2 capture

Results of the CO_2 adsorption capacities for both raw adsorbents and those modified with TEPA are listed in Table 2. For raw adsorbents, the pore size of ZSM-5 zeolite, 0.44 nm, is very similar to the molecular diameter of CO_2, 0.35 nm. Thus it can serve as a molecular sieve and has a much higher CO_2 adsorption capacity of 40 mg/g than the mesoporous adsorbents of MCM-41. However, when coated with TEPA, the small pore opening of ZSM-5 zeolite limited the access of TEPA molecules. Thus the excessive amount of TEPA reagents coated on the external surface would result in the blockage of the pore opening and the CO_2 capture could not be enhanced. Besides, TEPA-modified ZSM-5 zeolite had a gel-like morphology [25] and its surface area could not be measured. On the contrary, the TEPA-modified mesoporous silica materials, MCM-41(NaSi) and MCM-41(PWP), have larger pore sizes which would allow the loading of more TEPA molecules into the pore channels resulting in higher CO_2 capture capacities of 97 and 82 mg/g, respectively.

Fig. 10 displays the breakthrough curves of CO_2 over TEPA-modified adsorbents at 25 °C via the packed column reactor. Initially all adsorbents could have adsorption efficiencies of near 100%, but the breakthrough time of the TEPA/ZSM-5 zeolite adsorbent was the shortest, followed by the TEPA/MCM-41(PWP) and then the TEPA/MCM-41(NaSi). The slight difference in the CO_2 adsorption capacities between the TEPA/MCM-

Table 2
Physical properties and CO_2 adsorption capacities of photonic waste powder and mesoporous adsorbents.

Sample name	S_{BET}[a] (m^2/g)	D_p[b] (nm)	V_p[c] (cm^3/g)	Adsorption capacity (mg CO_2/g adsorbent)
Photonic waste powder	30	–	0.07	–
MCM-41(NaSi)	1102	3.0	1.13	4
MCM-41(PWP)	1082 ± 13	2.95 ± 0.05	0.99 ± 0.02	2
ZSM-5	361	0.44[d]	0.12[e]	40
TEPA/MCM-41(NaSi)	153	4.1	0.17	97
TEPA/MCM-41(PWP)	18	–[f]	0.12	82
TEPA/ZSM-5	–	–	–	43

[a] BET surface area.
[b] Pore diameter calculated by BJH theory.
[c] Pore volume calculated by BJH theory.
[d] Mean pore width calculated by Horvath–Kawazoe model.
[e] Pore volume calculated by *t*-plot method.
[f] Not detected.

41(NaSi) and TEPA/MCM-41(PWP) can be described by their N_2 adsorption–desorption isotherms as shown in Fig. 11 and their pore structure data listed in Table 2. Apparently, TEPA/MCM-41(NaSi) exhibited a better resolved capillary condensation step than that of TEPA/MCM-41(PWP). Thus the TEPA/MCM-41(NaSi)

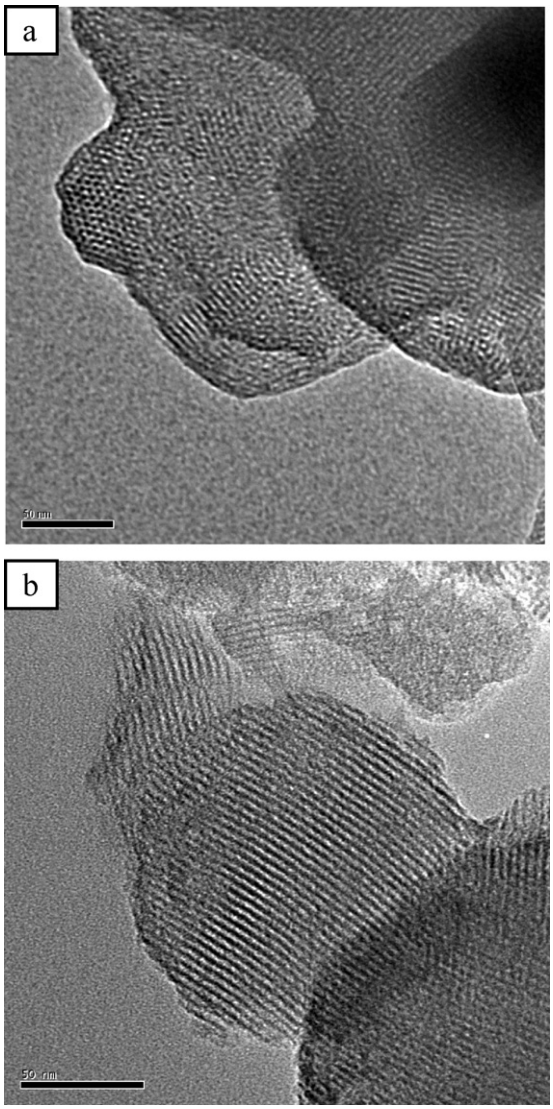

Fig. 9. TEM images of (a) MCM-41(NaSi) and (b) MCM-41(PWP). The scale bar in the TEM images is 50 nm.

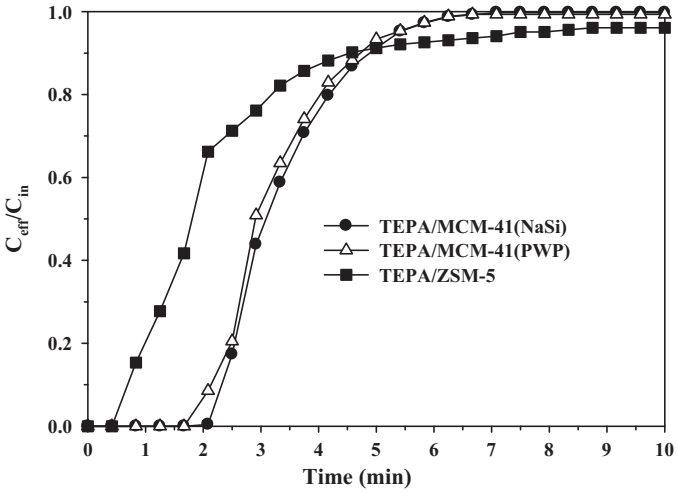

Fig. 10. CO_2 breakthrough curves for TEPA loaded adsorbents of MCM-41(NaSi), MCM-41(PWP) and ZSM-5 zeolite.

still maintained better a meso-structure as compared to that of TEPA/MCM-41(PWP). The density of TEPA is about 0.99 cm^3/g and the pore volumes of MCM-41(NaSi) and MCM-41(PWP) are 1.13 cm^3/g and 0.99 cm^3/g, respectively. Thus the maximum TEPA loading inside the pore channels was calculated to be 53% and 50%,

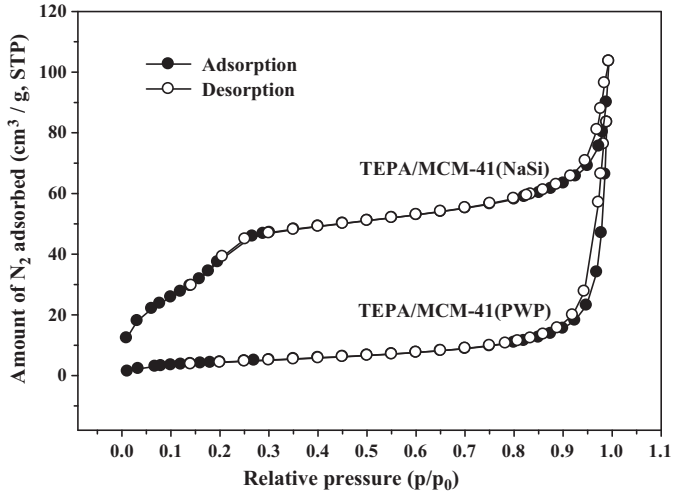

Fig. 11. N_2 adsorption–desorption isotherms of the TEPA/MCM-41(NaSi) and TEPA/MCM-41(PWP).

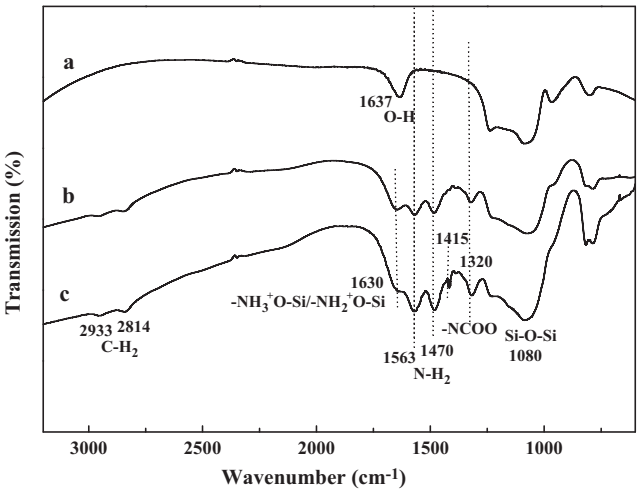

Fig. 12. FTIR spectra of (a) calcined MCM-41(PWP), (b) fresh TEPA/MCM-41(PWP), and (c) TEPA/MCM-41(PWP) after CO_2 adsorption.

respectively, for the MCM-41(NaSi) and MCM-41(PWP). As a result, the MCM-41(NaSi) had a higher CO_2 adsorption capacity due to the fact that it had a higher pore volume to accommodate TEPA molecules inside the pores. And as seen in Table 2, after loaded with TEPA, the BET surface area of the TEPA/MCM-41(NaSi) is higher than that of the TEPA/MCM-41(PWP).

The CO_2 adsorption mechanism could be described by the functional groups on the adsorbent surfaces as observed in the FTIR spectra shown in Fig. 12 for the MCM-41(PWP) (Fig. 12a) and fresh TEPA/MCM-41(PWP) (Fig. 12b). One can see that MCM-41(PWP) showed significant bands at 1637 and 1080 cm^{-1} corresponding to H–O–H band and Si–O–Si asymmetric stretching vibration, respectively. On the other hand, the FTIR spectrum of fresh TEPA/MCM-41(PWP) exhibited significant bands at 2933, 2814, 1630, 1563, 1470 and 1080 cm^{-1}. The bands at 2933 and 2814 cm^{-1} are related to C–H_2 stretching from $CH_2CH_2CH_2$–NH_2 (RNH_2), while 1563 and 1470 cm^{-1} can be assigned to N–H_2 vibration in the primary amine group (RNH_2) [6]. And the band at 1630 cm^{-1} can be assigned to the NH_3^+ deformation of the protonated primary amine group or secondary amine group (–NH_3^+O–Si/–NH_2^+O–Si). The presence of the C–H, N–H_2 and –NH_3^+O–Si/–NH_2^+O–Si confirms that TEPA was successfully grafted on the surface of MCM-41(PWP). Additionally, the spectrum of TEPA/MCM-41(PWP) after CO_2 adsorption test was also measured (Fig. 12c). It was observed that one distinguished band appeared at 1415 cm^{-1} which can be corresponded to the NCOO skeletal vibration, indicating the formation of alkylammonium carbamate through the CO_2 adsorption process. Generally, the following chemical reactions are expected to take place when CO_2 molecules react with TEPA [26]:

$$CO_2 + 2RNH_2 \rightarrow RNHCOO^- + RNH_3^+ \quad (4)$$

$$CO_2 + 2R_1R_2NH \rightarrow R_1NHCOO^- + R_2NH_2^+ (\text{or} R_2NCOO^- + R_1NH_2^+) \quad (5)$$

$$CO_2 + R_2NH + RNH_2 \rightarrow R_2NCOO^- + RNH_3^+ (\text{or} RNHCOO^- + R_2NH_2^+) \quad (6)$$

4. Conclusions

This study successfully demonstrated the feasibility of recycling the photonic waste powder to avoid the fast drain of the natural resources. It can be employed for the Si-related industries such as semiconductor, opto-electronic and solar cell industries as a waste reduction strategy. It was confirmed that alkali fusion at the temperature of 550 °C is a viable process which can effectively separate the silicate species from the waste powder. The extracted sodium silicate was capable of replacing commercial silica precursor for the production of mesoporous MCM-41 material with high surface area (1082 cm^2/g) and large pore volume (0.99 cm^3/g). Meanwhile, near purified sodium fluoride (>90%) was also obtained as the sediment during the extraction process, which can also be a valuable resource of fluoride. As a result, two valuable products were produced during the waste recovery process. Adsorption breakthrough experiments confirmed that amine-modified MCM-41(PWP), with a high adsorption capacity of 82 mg CO_2/g adsorbent, can be used as an effective adsorbent to reduce CO_2 greenhouse gas emission.

Acknowledgments

The authors gratefully acknowledge the financial support from the National Science Council of the Republic of China through Grant No.: NSC 98-2221-E-009-023-MY3.

References

[1] S. Liu, C. Wu, H. Lee, S. Liu, Highly stable amine-modified mesoporous silica materials for efficient CO_2 capture, Top. Catal. 53 (2010) 210–217.
[2] C.T. Kresge, M.E. Leonowicz, W.J. Roth, J.C. Vartuli, J.S. Beck, Ordered mesoporous molecular sieves synthesized by a liquid-crystal template mechanism, Nature 359 (1992) 710–712.
[3] Z. Bian, Y. Huo, Y. Zhang, J. Zhu, Y. Lu, H. Li, Aerosol-spay assisted assembly of $Bi_2Ti_2O_7$ crystals in uniform porous microspheres with enhanced photocatalytic activity, Appl. Catal. B: Environ. 91 (2009) 247–253.
[4] X. Wang, V. Schwartz, J.C. Clark, X. Ma, S.H. Overbury, X. Xu, C. Song, Infrared study of CO_2 sorption over "molecular basket" sorbent consisting of polyethylenimine-modified mesoporous molecular sieve, J. Phys. Chem. C 113 (2009) 7260–7268.
[5] N. Baccile, D. Grosso, C. Sanchez, Aerosol generated mesoporous silica particles, J. Mater. Chem. 13 (2003) 3011–3016.
[6] L. Lin, H. Bai, Continuous generation of mesoporous silica particles via the use of sodium metasilicate precursor and their potential for CO_2 capture, Microporous Mesoporous Mater. 136 (2010) 25–32.
[7] K. Hui, C. Chao, Synthesis of MCM-41 from coal fly ash by a green approach: influence of synthesis pH, J. Hazard. Mater. 137 (2006) 1135–1148.
[8] M. Bhagiyalakshmi, L.J. Yun, R. Anuradha, H.T. Jang, Utilization of rice husk ash as silica source for the synthesis of mesoporous silicas and their application to CO_2 adsorption through TREN/TEPA grafting, J. Hazard. Mater. 175 (2010) 928–938.
[9] H. Chang, C. Chun, I.A. Aksay, W. Shih, Conversion of fly ash into mesoporous aluminosilicate, Ind. Eng. Chem. Res. 38 (1999) 973–977.
[10] C.L. Choi, M. Park, D.H. Lee, J. Kim, B. Park, J. Choi, Salt-thermal zeolitization of fly ash, Environ. Sci. Technol. 35 (2001) 2812–2816.
[11] M. Bhagiyalakshmi, J.Y. Lee, H.T. Jang, Synthesis of mesoporous magnesium oxide: its application to CO_2 chemisorption, Int. J. Greenh. Gas Control. 4 (2010) 51–56.
[12] M. Karthik, L. Lin, H. Bai, Bifunctional mesoporous Cu–Al-MCM-41 materials for the simultaneous catalytic abatement of NOx and VOCs, Microporous Mesoporous Mater. 117 (2009) 153–160.
[13] C. Lu, H. Bai, F. Su, W. Chen, J.F. Hwang, H. Lee, Adsorption of carbon dioxide from gas streams via mesoporous spherical-silica particles, J. Air Waste Manage. Assoc. 60 (2010) 489–496.
[14] M. Saadoun, B. Bessaïs, N. Mliki, M. Ferid, H. Ezzaouia, R. Bennaceur, Formation of luminescent $(NH_4)_2SiF_6$ phase from vapour etching-based porous silicon, Appl. Surf. Sci. 210 (2003) 240–248.
[15] C. Lu, H. Bai, B. Wu, F. Su, J.F. Hwang, Comparative study of CO_2 capture by carbon nanotubes, activated carbons, and zeolites, Energ. Fuel 22 (2008) 3050–3056.
[16] H.S Yu, K. Rhee, C.K. Lee, D. Yang, Two-step ammoniation of by-product fluosilicic acid to produce high quality amorphous silica, Korean J. Chem. Eng. 17 (2000) 401–408.
[17] E.I. Mel'nichenko, G.F. Krysenko, M.N. Mel'nichenko, $(NH_4)_2SiF_6$ evaporation in the presence of SiO_2, Russ. J. Inorg. Chem. 51 (2006) 27–31.
[18] T. Cardinal, O. Efimov, H. Francois-Saint-Cyr, L. Glebov, L. Glebova, V. Smirnov, Comparative study of photo-induced variations of X-ray diffraction and refractive index in photo-thermo-refractive glass, J. Non-Cryst. Solids 325 (2003) 275–281.
[19] P.B. Sarawade, J. Kim, A. Hilonga, H.T. Kim, Recovery of high surface area mesoporous silica from waste hexafluorosilicic acid (H_2SiF_6) of fertilizer industry, J. Hazard. Mater. 173 (2010) 576–580.
[20] L. Wang, A. Lu, C. Wang, X. Zheng, D. Zhao, R. Liu, Nano-fibriform production of silica from natural chrysotile, J. Colloid Interface Sci. 295 (2006) 436–439.

[21] K. Liu, Q. Feng, Y. Yang, G. Zhang, L. Ou, Y. Lu, Preparation and characterization of amorphous silica nanowires from natural chrysotile, J. Non-Cryst. Solids 353 (2007) 1534–1539.
[22] C. Hung, H. Bai, M. Karthik, Ordered mesoporous silica particles and Si-MCM-41 for the adsorption of acetone: a comparative study, Sep. Purif. Technol. 64 (2009) 265–272.
[23] M.T. Bore, S.B. Rathod, T.L. Ward, A.K. Datye, Hexagonal mesostructure in powders produced by evaporation-induced self-assembly of aerosols from aqueous tetraethoxysilane solutions, Langmuir 19 (2003) 256–264.
[24] G. Chandrasekar, K. You, J. Ahn, W. Ahn, Synthesis of hexagonal and cubic mesoporous silica using power plant bottom ash, Microporous Mesoporous Mater. 111 (2008) 455–462.
[25] M.B. Yue, L. Sun, Y. Cao, Y. Wang, Z. Wang, J. Zhu, Efficient CO_2 capturer derived from as-synthesized MCM-41 modified with amine, Chem. Eur. J. 14 (2008) 3442–3451.
[26] X. Wang, H. Li, H. Liu, X. Hou, AS-synthesized mesoporous silica MSU-1 modified with tetraethylenepentamine for CO_2 adsorption, Microporrous Mesoporous Mater. 142 (2011) 564–569.